

Chinese Pharmaceutical Association
Institute of Materia Medica, Chinese Academy of Medical Sciences

Acta Pharmaceutica Sinica B

www.elsevier.com/locate/apsb www.sciencedirect.com



ORIGINAL ARTICLE

Cannabidiol alleviates methamphetamine addiction *via* targeting ATP5A1 and modulating the ATP-ADO-A1R signaling pathway



Sha Jin^{a,b,c,†}, Cong Lin^{a,*,†}, Peipei Li^{d,†}, Xue Wang^e, Yibo Wang^a, Cong Zhang^a, Xuenan Wang^d, Yinghua Peng^f, Haohong Li^g, Yuyuan Lu^{c,h,*}, Xiaohui Wang^{a,c,i,*}

Received 13 November 2024; received in revised form 17 April 2025; accepted 17 June 2025

KEY WORDS

Cannabidiol; Methamphetamine; Addiction; **Abstract** Cannabidiol (CBD), a non-psychoactive cannabinoid, shows great promise in treating methamphetamine (METH) addiction. Nonetheless, the molecular target and the mechanism through which CBD treats METH addiction remain unexplored. Herein, CBD was shown to counteract METH-induced locomotor sensitization and conditioned place preference. Additionally, CBD mitigated the

Peer review under the responsibility of Chinese Pharmaceutical Association and Institute of Materia Medica, Chinese Academy of Medical Sciences.

^aLaboratory of Chemical Biology, Changchun Institute of Applied Chemistry, Chinese Academy of Sciences, Changchun 130022, China

^bDepartment of Chemistry and Chemical Engineering, Hunan Institute of Science and Technology, Yueyang 414000, China

^cSchool of Applied Chemistry and Engineering, University of Science and Technology of China, Hefei 230026, China

^dShandong Institute of Brain Science and Brain-inspired Research, Shandong First Medical University & Shandong Academy of Medical Sciences, Jinan 250117, China

^eDepartment of Anesthesiology, Lequn Branch, the First Hospital of Jilin University, Changchun 130021, China ^fState Key Laboratory for Molecular Biology of Special Economic Animal, Institute of Special Animal and Plant Sciences, Chinese Academy of Agricultural Sciences, Changchun 130112, China

^gThe MOE Frontier Research Center of Brain and Brain-Machine Integration, Zhejiang University School of Brain Science and Brain Medicine, Hangzhou 310058, China

^hState Key Laboratory of Polymer Physics and Chemistry, Changchun Institute of Applied Chemistry, Chinese Academy of Sciences, Changchun 130022, China

ⁱState Key Lab of Brain-Machine Intelligence, Zhejiang University, Hangzhou 311121, China

^{*}Corresponding authors.

E-mail addresses: cong.lin@ciac.ac.cn (Cong Lin), yylu@ciac.ac.cn (Yuyuan Lu), xiaohui.wang@ciac.ac.cn (Xiaohui Wang).

[†]These authors made equal contributions to this work.

Mitochondria; ATP5A1; ATP synthetase; Adenosine triphosphate; Adenosine A1 receptor adverse effects of METH, such as cristae loss, a decline in ATP content, and a reduction in membrane potential. Employing an activity-based protein profiling approach, a target fishing strategy was used to uncover CBD's direct target. ATP5A1, a subunit of ATP synthase, was identified and validated as a CBD target. Moreover, CBD demonstrated the ability to ameliorate METH-induced ubiquitination of ATP5A1 via the D376 residue, thereby reversing the METH-induced reduction of ATP5A1 and promoting the assembly of ATP synthase. Pharmacological inhibition of the ATP efflux channel pannexin 1, blockade of ATP hydrolysis by a CD39 inhibitor, and blocking the adenosine A1 receptor (A1R) all attenuated the therapeutic benefits of CBD in mitigating METH-induced behavioral sensitization and CPP. Moreover, the RNA interference of ATP5A1 in the ventral tegmental area resulted in the reversal of CBD's therapeutic efficacy against METH addiction. Collectively, these data show that ATP5A1 is a target for CBD to inhibit METH-induced addiction behaviors through the ADO—A1R signaling pathway.

© 2025 The Authors. Published by Elsevier B.V. on behalf of Chinese Pharmaceutical Association and Institute of Materia Medica, Chinese Academy of Medical Sciences. This is an open access article under the CC BY-NC-ND license (http://creativecommons.org/licenses/by-nc-nd/4.0/).

1. Introduction

Methamphetamine (METH), a synthetic psychostimulant, causes use disorders^{1,2} and overdose-related fatalities³, imposing significant societal economic and mental health burdens. METH exposure leads to significant dopamine accumulation at synaptic clefts⁴, producing reactive oxygen species *via* oxidation⁵, resulting in mitochondrial dysfunction⁶⁻⁸. This dysfunction is increasingly understood to be pivotal in the progression of METH addiction^{9,10}. Adenosine triphosphate (ATP), while mainly recognized as an intracellular energy molecule, also has extracellular functions, acting as neurotransmitters when in the form of ATP or its metabolite adenosine (ADO), affecting psychiatric conditions and drug addiction ¹¹⁻¹⁴. The ATP synthase F1 subunit alpha (ATP5A1) protein, a component of the ATP synthesizing machinery, has shown reduced expression in various addiction models, positing it as a potential addiction biomarker 15,16, suggesting it might be a valuable target for addressing METH addiction.

Cannabidiol (CBD), a primary active compound in cannabis, has been explored for its potential therapeutic properties in several neuropsychiatric conditions, including substance use disorders caused by various psychostimulants ^{17,18}. The potential therapeutic effects of CBD on METH addiction have garnered attention in recent years. CBD can reduce METH-induced hyperactivity and conditioned place preference (CPP), suggesting its potential in reducing METH-seeking behavior and the risk of relapse 19,20. Recent studies reveal CBD's influence on ATP, a pivotal molecule in cellular energy metabolism and in the regulation of mitochondrial function. CBD effectively restores mitochondrial function and reduces oxidative stress, thereby treating pulmonary arterial hypertension²¹. In Alzheimer's disease, CBD activates TRPV2 channels, enhancing microglial clearance of amyloid-β and boosting ATP production to reduce neuroinflammation²². Additionally, CBD protects against oxidative stress and inflammation by optimizing astrocytic mitochondrial function, suggesting its potential in treating metabolic and neuroinflammatory disorders²³. Nonetheless, the possible mechanisms underlying the therapeutic potential of CBD in METH use disorders through mitochondrial function-related pathways remain to be fully elucidated. In this study, ATP5A1 was identified as the direct target of CBD. CBD enhanced ATP synthesis by improving ATP5A1 expression and assembly, leading to increased ATP

production, especially in the ventral tegmental area (VTA). The subsequent release and metabolism of this ATP into ADO potentially disrupted METH-induced behavioral sensitization and CPP through the adenosine A1 receptor (A1R) signaling pathway. These results suggest that ATP5A1 is a promising therapeutic target for METH addiction.

2. Materials and methods

2.1. Materials

Chemicals and reagents were purchased from Energy Chemical (Supporting Information Table S1) unless otherwise stated. CBD was dissolved in 5% DMSO, 7% Tween 80, and 88% saline. The antibodies with the indicated dilutions were as follows: ATP5A1 (Proteintech, Wuhan, China, 66037-1-Ig, 1:10,000; Affinity, Suzhou, China, DF3806, 1:100; Invitrogen, Carlsbad, CA, USA, 7H10BD4F9, 1:100); ATP5B (Proteintech, 66600-1-Ig, 1:10,000); ATP5C1 (Proteintech, 10910-1-AP, 1:2000); Ubiquitin (P37) (Cell Signaling Technology, Danvers, MA, USA, 58395, 1:2000); β actin (Proteintech, 66009-1-Ig, 1:10,000); Mouse IgG (Bioworld, Beijing, China, BD0050); GluA1 (Cell Signaling Technology, 13185, 1:2000); Phospho-GluA1 (Cell Signaling Technology, 8084, 1:1000); Flag (Proteintech, 66008-4-Ig, 1:5000); HA (Proteintech, 66006-2-Ig, 1:5000); HRP-conjugated Goat Anti-Mouse IgG (H + L) (Proteintech, SA00001-1, 1:2000), HRP-conjugated Goat Anti-Rabbit IgG (H + L) (Proteintech, SA00001-2, 1:2000); Alexa Fluor 488 Goat Anti-Mouse IgG H&L (Abcam, Cambridge, UK, ab150113, 1:200); Alexa Fluor 647 Goat Anti-Mouse IgG H&L (Abcam, ab150115, 1:200).

2.2. Animals

BABL/c male mice (6–8 weeks, 20–28 g) were purchased from Liaoning Changsheng Biotechnology Co., Ltd. Mice were maintained at animal facility with temperature of 21–25 °C, humidity of 40%–60% and light-controlled (12 h light: dark cycle; lights on at 8:00). Mice were fed with standard rodent food and water and allowed to eat and drink freely. Mice were allowed to habituate to the environment for at least 1 week before experimentation. All

the animal experiments were approved by the Institutional Animal Care and Use Committee (Protocol No. CIAC2022-0055).

2.3. Behavioral sensitization experiment

The behavioral sensitization experiment was conducted according to previous literature with some modifications 24 . Mice were placed into the open field ($40~\rm cm \times 40~\rm cm \times 40~\rm cm$) for 1 h to habituate the devices during the first 3 days. Behavioral sensitization tests were carried out for 7 consecutive days. Mice were placed into the open field for 1 h after daily injections of METH (1 mg/kg, i.p.), CBD (i.p.), or the combination of METH (1 mg/kg) with CBD, and the moving traces were recorded. After a 7-day withdrawal period, mice were challenged by METH (0.5 mg/kg, i.p.) to assess behavioral sensitization. The subsequent recordings of the moving traces were used to evaluate the sustained therapeutic effects of CBD.

2.4. Conditional place preference procedures (CPP)

CPP was performed on a 12-day protocol²⁵. Briefly, mice were placed separately in the CPP apparatus for 15 min on the first two days to habituate the devices. On the 3rd day (preconditioning), mice were allowed to explore freely in the device for 15 min, and the moving traces were recorded. The time spent in each compartment was analyzed to determine the preference of the mice. The compartment where mice spent less time is the paired compartment for METH treatment. The preconditioning data were shown in Supporting Information Tables S2-S4. Mice were divided into six groups: vehicle group, CBD (50 mg/kg) group, METH (2 mg/kg) group, METH (2 mg/kg) + CBD (2 mg/kg) group, METH (2 mg/kg) + CBD (20 mg/kg) group and METH (2 mg/kg) + CBD (50 mg/kg) group. The CPP training lasted 8 days and had a total of 4 cycles. Mice were separately isolated in the compartment for 30 min after daily treatment. Mice were administrated with METH (2 mg/kg, i.p.) on Days 3, 5, 7, 9, and administrated with vehicle (5 mL/kg saline, i.p.) on Days 4, 6, 8, 10. The indicated doses of CBD were given daily along the administration with METH or vehicle. The CPP test was performed 24 h after the last training. Mice were allowed to explore freely in the device, and the moving traces were recorded for 15 min. The CPP scores (s) were calculated by the time spent in the METH-paired compartment minus the time spent in the vehicle-paired compartment.

2.5. Electron microscopy

Mice were sacrificed, and the brains were collected and blocked with 2.5% glutaraldehyde for 1 day. Tissues were fixed with 2.5% (v/v) glutaraldehyde and 2% paraformaldehyde (v/v) in Phosphate Buffer (PB) (0.1 mol/L, pH 7.4), washed twice in PB and twice in ultrapure water. Then, the samples were first immersed in an aqueous solution of 1% (w/v) OsO₄ and 1.5% (w/v) potassium ferricyanide at 4 °C for 2 h. After washing, tissues were dehydrated through a graded series of alcohols (30%, 50%, 70%, 80%, 90%, 100%, 10 min each) and then into pure acetone $(2 \times 10 \text{ min})$. Samples were infiltrated in a graded mixture (3:1, 1:1, 1:3) of acetone and SPI-PON812 resin (19.6 mL SPI-PON812, 6.6 mL DDSA, and 13.8 mL NMA), then changed to pure resin. Finally, tissues were embedded in pure resin with 1.5% BDMA and polymerized for 12 h at 45 °C, 48 h at 60 °C. The ultrathin sections (70 nm thick) were sectioned with a microtome

(Leica EM UC6), double-stained with uranyl acetate and lead citrate, and examined by a transmission electron microscope (FEI Tecnai Spirit120 kV) with the EMSIS CCD camera (VELETA)

2.6. Measurement of mitochondrial membrane potential

The mitochondrial membrane potential ($\Delta\psi_{m}$) was assessed using the JC-1 assay kit (Beyotime Biotechnology Co., Ltd., C2006, China). Mice were subjected to daily administrations of METH (2 mg/kg), CBD (50 mg/kg), or a combination of METH (2 mg/kg) + CBD (50 mg/kg). Following 14 days of treatment, the mice were sacrificed, and the VTA regions were collected and homogenized. Mitochondria were isolated using a commercial mitochondria isolation kit (Beyotime, Shanghai, China, C3606) and incubated with JC-1 dye according to the standard protocol. $\Delta\psi_{m}$ was measured by a SYNERGY H1 Microplate Reader (BioTek Instruments, Carlsbad, CA, USA).

2.7. ATP measurement

ATP was measured by an enhanced ATP assay kit (Beyotime, S0027-4). Mice were subjected to daily administrations of METH (2 mg/kg), CBD (50 mg/kg), or a combination of METH (2 mg/kg) + CBD (50 mg/kg) over 14 days. Mice were sacrificed 24 h after the last injection. The medial prefrontal cortex (mPFC), nucleus accumbens (NAc), and VTA regions were collected, and the homogenates were prepared with ATP lysate added to 2% perchloric acid. Protein concentration was measured using a bicinchoninic acid (BCA) protein quantification kit (20201ES86, YEASEN, Shanghai, China).

2.8. In situ pull-down analysis for the identification of the target protein

BV-2 cells were treated with the probe CP1 (10 µmol/L) in the presence or absence of 60 µmol/L CBD for 2 h at 37 °C. Cells were treated with the probe CP2 (10 μmol/L) for 2 h at 37 °C as a control. Subsequently, the cells were placed on ice and irradiated with 365-nm UV light for 30 min. After washing twice with 3 mL of PBS (137 mmol/L NaCl, 2.7 mmol/L KCl, 10 mmol/L Na₂HPO₄, 1.8 mmol/L KH₂PO₄, pH = 7.4), cells were lysed using a buffer containing 25 mmol/L HEPES (pH = 8.0), 150 mmol/L KCl, 5 mmol/L EDTA, 0.5% NP-40, and 1% protease inhibitor cocktail. The lysates were centrifuged at 4 °C for 10 min at $12,000 \times g$, and the protein concentration was adjusted to 1 mg/mL using the BCA assay kit. The click reaction was carried out using 80 µmol/L biotin-N3, 100 µmol/L TBTA, 1 mmol/L TCEP, 1 mmol/L CuSO₄, and 5% t-BuOH at room temperature for 1 h. The proteins were captured with 20 μL streptavidin magnetic beads (Invitrogen, 11206D) and mixed with 50 µL of $2 \times$ Laemmli buffer, then incubated at 100 °C for 8 min. The samples were separated using SDS-PAGE and subjected to silver staining (Beyotime, P0017S). Bands were cut, and the proteins were then identified using LC-MS/MS analysis.

2.9. Immunoblotting

The protein samples underwent separation by SDS-PAGE and were then transferred onto PVDF membranes (IPVH00010, Merck Millipore, Darmstadt, Germany). The membranes were blocked with 5% nonfat dry milk for 1 h. Next, membranes were incubated with the specific primary antibody at 4 °C overnight. After

primary antibody incubation, membranes were washed 3 times in Tris-buffered saline containing 0.1% Tween 20 (TBST) for 5 min each time. Membranes were finally incubated with the secondary HRP-conjugated antibody for at least 1 h at room temperature. After washing with TBST, proteins were detected using the Super ECL Detection Reagent (36208ES76, YEASEN) and were imaged using the Tanon-5200 Multi system. Densitometric analysis was performed using ImageJ.

2.10. Cellular thermal shift assay (CETSA)

BV-2 cells were initially seeded at a density of 4×10^5 cells/mL in the 10 cm dish. After incubation for 24 h, the medium was removed and the cells were washed three times with cold PBS. Subsequently, cells were harvested through scraping and isolated by centrifugation (1000 \times g, 5 min, 4 °C). The cell pellet was resuspended in cell lysis buffer (P0013, Beyotime) containing 1% protease inhibitor cocktail and lysed on ice for 10 min. The lysates were centrifuged at $12,000 \times g$ for 15 min at 4 °C to collect the supernatants. The lysate supernatants were incubated with either 100 $\mu mol/L$ CBD or vehicle control (DMSO) for 2 h at 20 $^{\circ}C.$ The lysate supernatants were divided into 60 µL in each microtube, and then heated to different temperatures (ranging from 48 to 60 °C) for 5 min using an A200 thermal cycler (Long Gene, Shanghai, China) and cooled down to 25 °C for another 3 min. The samples were centrifuged at $20,000 \times g$ for 20 min at 4 °C to remove precipitates. The supernatant samples were denatured in 2 \times Laemmli sample buffer at 100 °C for 8 min for Western blotting analysis with the ATP5A1 antibody.

2.11. Protein expression and purification

Full-length wild-type ATP5A1 and ATP5A1 D376A mutant mouse protein were expressed as a $6 \times \text{His}$ -tagged fusion protein in *E. coli* strain BL21, induced with 1 mmol/L IPTG for 4 h at 30 °C, and subsequently purified using High Affinity Ni-Charged Resin (L00250-100, GenScript, Nanjing, China) according to the manufacturer's instructions.

2.12. Protein thermal shift assay

The protein thermal shift assay was performed using 0.1 μ mol/L of purified ATP5A1 or ATP5A1 D376A protein, following the same protocol described above for CESTA.

2.13. Fluorescence titration

Fluorescence titration assay was measured by a previously reported method 26 . The ATP5A1 protein (0.5 $\mu mol/L$) was titrated with increasing concentrations of CBD (0.5–80 $\mu mol/L$), and the fluorescence intensity ($\lambda_{ex}=280$ nm; $\lambda_{em}=337$ nm) was recorded using a Cary Eclipse spectrophotometer (Agilent Technologies, Santa Clara, CA, USA). The fluorescence intensity was plotted against CBD concentrations for fitting the dissociation constant.

2.14. ATP synthetase activity measurement

The ATP synthetase activity was determined using a MitoTox Complex V OXPHOS activity assay kit (Abcam, ab109907) according to standard procedures. Briefly, various concentrations of CBD or METH (0.001 to 200 µmol/L) were incubated with pre-

coated bovine heart mitochondria in a 96-well plate for 45 min at 37 °C. Following the incubation, complex V activity buffer was added, and the absorption at 340 nm was measured every minute for 60 min. The ATP synthetase activity was then calculated using the following Eqs. (1) and (2):

Complex
$$V$$
 activity = $Rate_{sample} - Rate_{background}$ (1)

Reaction Rate
$$(OD/min) = (OD_2 - OD_1)/(T_2 - T_1)$$
 (2)

OD represents the absorption at 340 nm, and T represents the test time.

2.15. Molecular docking

The ATP synthase protein was extracted from the crystal structure of the bovine F1-c8 sub-complex of ATP synthase (PDB: 2XND)²⁷. Missing residues and hydrogen atoms were repaired at pH 7.0 using Maestro²⁸. The molecular structure of CBD was obtained from PubChem. Semiflexible molecular docking was carried out using AutoDock Vina 1.2.3^{29,30}.

2.16. Immunofluorescence staining

Mice were anesthetized with 0.6 mL 2% tribromoethanol following the 14-day administration and then intracardially perfused with 7 mL of saline and 7 mL 4% paraformaldehyde (4% PFA) to remove blood. The brains were subsequently collected and soaked in 4% PFA overnight, and then transferred to 30% sucrose solution. After 36 h, coronal brain sections (40 µm thick) were obtained using a cryostat. Coronal brain sections were then placed in 0.01 mol/L citrate buffer (pH 6.0) and subjected to antigen retrieval by heating in a microwave oven. Following incubation with 3% bovine serum protein at 37 °C for 2 h, the sections were incubated overnight at 4 °C with primary antibodies. After washing three times with PBS, the sections were incubated with secondary antibodies in the dark for 1 h. Finally, the sections were washed twice with PBS for 5 min each time, counterstained with DAPI, and examined using a laser confocal microscope (Zeiss, Oberkochen, GER).

2.17. *qRT-PCR*

Total RNA was extracted from the VTA of mice via the TRIzol reagent (15596026, Invitrogen). Isolated RNA was reverse-transcribed into cDNA using a reverse transcription kit (22106, TOLOBIO, Shanghai, China) following the standard procedure. Subsequently, the cDNA was subjected to PCR amplification using synthetic primers and SYBR Green (11201ES03, YEASEN) on a TOptical Real-Time qPCR Thermal Cycler (Analytik Jena, Thuringia, Germany). The resulting data were analyzed utilizing the $\Delta\Delta$ Ct method with Rpl7l1 serving as the internal control. Primer sequences used for RT-qPCR was showed in Supporting Information Table S5.

2.18. Co-immunoprecipitation

The VTA of mice was collected using a brain matrix (68713, RWD, Shenzhen, China). The VTA was homogenized and then lysed in 0.2 mL of lysate buffer containing 25 mmol/L Tris-HCl (pH = 8.0), 150 mmol/L KCl, 5 mmol/L EDTA, 0.5% NP-40, and 1% protease inhibitor cocktail on ice for 30 min. The supernatant was collected by centrifuging at $12,000 \times g$ for 15 min at 4 °C and

adjusting the protein concentration to 0.5 mg/mL using a BCA kit (20201ES86, YEASEN). Next, 1 mL of the supernatant was added to either 3 μg of the anti-ATP5A1 antibody or the anti-IgG antibody and incubated overnight at 4 °C. After incubation, the supernatant was mixed with 20 μL of protein A/G magnetic beads (HY-K0202, MedChemExpress, Monmouth Junction, USA). Following a 1.5 h incubation, the beads were washed three times with PBS, and then denatured in 40 μL 2 \times Laemmli sample buffer at 100 °C for 8 min for Western blotting.

2.19. Cycloheximide (CHX) chase assay for determining protein half-life

HEK293T cells with a confluence rate about 50% in 10 cm dishes were co-transfected with 10 μg of Flag-ATP5A1 or Flag-ATP5A1 D376A, 10 μg of HA-ubiquitin plasmids, and 10 μg of polyethylenimine (PEI), followed by 8 h of incubation. The medium was then replaced with DMEM (10% FBS, 1% PS) and the cells were cultured for 48 h. Subsequently, the transfected HEK293T cells were sub-cultured at a ratio of 1:4. After 24 h, the cells were treated with 50 $\mu g/mL$ CHX (MedChemExpress, HY-12320) and 10 $\mu mol/L$ CBD. After a period of incubation, the cells were harvested using a cell scraper and lysed with cell lysis buffer (Beyotime, P0013) containing 1% protease inhibitor cocktail. Immunoblotting was carried out.

2.20. Determination of ATP5A1 ubiquitination levels

Transfected HEK293T cells were treated with 10 μ mol/L MG132 (MedChemExpress, HY-13259) and 10 μ mol/L CBD for 8 h, then harvested using a cell scraper. Co-immunoprecipitation procedures were performed according to the protocol established for brain tissue samples, using a Flag antibody.

2.21. Blue native electrophoresis and immunoblotting

Mitochondria were isolated using a tissue mitochondria isolation kit (C3606, Beyotime) according to the standard procedure. Mitochondria from mice were resuspended in 40 µL lysate buffer (50 mmol/L NaCl, 50 mmol/L imidazole, 2 mmol/L 6aminoheptanoic acid, pH = 7.0, 5% digitonin) per 400 μg protein, and then lysed for 10 min on ice. The supernatant was collected by centrifuging at $20,000 \times g$ for 20 min at 4 °C. 1 µL of 5% Coomassie Brilliant Blue G-250, 5 μL of 50% glycerol, and 15 μL of BN-PAGE loading buffer (PL114, Real-Times, Beijing, China) were added per 400 µg of protein. The final mixtures (10 μL/well for silver staining, 5 μL/well for immunoblotting) were subjected to electrophoresis using a native 3%-12% Bis-tris gel (RTD6138-0312, Real-Times). The gel was then subjected to silver staining using a fast silver stain kit (Beyotime, P0017S) after electrophoresis. The proteins in the gel could also be transferred by electroblotting onto a PVDF membrane after electrophoresis, and then detected by anti-ATP5A1 antibody.

2.22. Adeno-associated virus (AAV) injection

AAV9-shATP5A1-CMV-EGFP-WPRE and AAV9-CMV-EGFP-WPRE were obtained from OBiO Technology (Shanghai, China); rAAV-EF1 α -ATP1.0 was purchased from Brain Case (Shenzhen, China). Stereotaxic injections into the VTA were performed at coordinates: antero-posterior -3.16 mm, mediolateral ± 0.50 mm, dorso-ventral -4.50 mm relative to bregma.

A microsyringe pump system (RWD, R480) delivered viral vectors at 200 nL/min, with the needle retained for 10 min post-injection. For RNA interference experiments, 500 nL of AAV9 was administered (250 nL per hemisphere). Unilateral injections of 100 nL were used for ATP content assays.

2.23. Statistical analysis

Data are expressed as mean \pm standard error of mean (SEM). Statistical analysis was done by the GraphPad Prism version 9.5 (GraphPad Software). Behavioral sensitization data were analyzed by paired *t*-test, and other data were analyzed by one-way ANOVA. Gene ontology analysis was performed using the DAVID bioinformatics database, and all proteins were clustered based on cellular components.

3. Results

3.1. CBD alleviates METH-induced addiction behaviors and mitochondrial damage

METH is a potent central nervous system (CNS) stimulant and has a high potential for misuse and addiction³¹. The potential therapeutic effects of CBD on METH addiction have garnered attention in recent years³². To confirm the therapeutic effect of CBD on METH-induced behavior, the locomotor sensitization assay was first performed (Supporting Information Fig. S1A). Following daily repeated METH exposure, the mice showed progressively increasing locomotor activity from Day 1 to Day 7 when compared to the saline-treated vehicle group (Fig. 1A). CBD attenuated METH-induced locomotor activity increase during the first 7 days in a dose-dependent manner (Fig. 1A), while CBD (50 mg/kg) alone did not produce any effect on locomotor activity. Following 1 week of withdrawal (Days 8-14), mice were challenged with 1 mg/kg METH on Day 15. METH challenge significantly induced the expression of behavioral sensitization in METH-pretreated mice (Fig. 1A). CBD decreased the behavioral sensitization to the METH challenge in a dose-dependent manner (Fig. 1A). These results show that CBD suppresses the development and expression of METH-induced behavioral sensitization. CPP is a standard behavioral model for measuring the rewarding effect of drugs (Fig. S1B). Mice exhibited a preference, as reflected by spending more time in the environment paired with METH after an 8-day training (Fig. 1B). Administration of CBD decreased the mice preference for METH in a dose-dependent manner (Fig. 1B). Together, these data show CBD alleviates METH-induced locomotor sensitization and CPP, suggesting its potential in reducing METH-seeking behavior.

Chronic METH use leads to persistent feelings of fatigue and exhaustion³³. Given the crucial role in cellular energy production, mitochondria are considered an essential organelle in the context of cellular damage induced by METH. Therefore, the relationship between METH and mitochondrial dysfunction provides a potential avenue for therapeutic intervention to counteract some of the deleterious effects of METH. Mice received a daily dose of either METH (2 mg/kg), CBD (50 mg/kg), or a combined treatment of METH (2 mg/kg) + CBD (50 mg/kg). Over 14 days, mice were sacrificed, and the mPFC, NAc, and VTA regions, which play a pivotal role in METH-induced reward circuitry in the CNS, were dissected. The morphology of mitochondria in mPFC, NAc, and VTA was assessed using transmission electron microscopy.

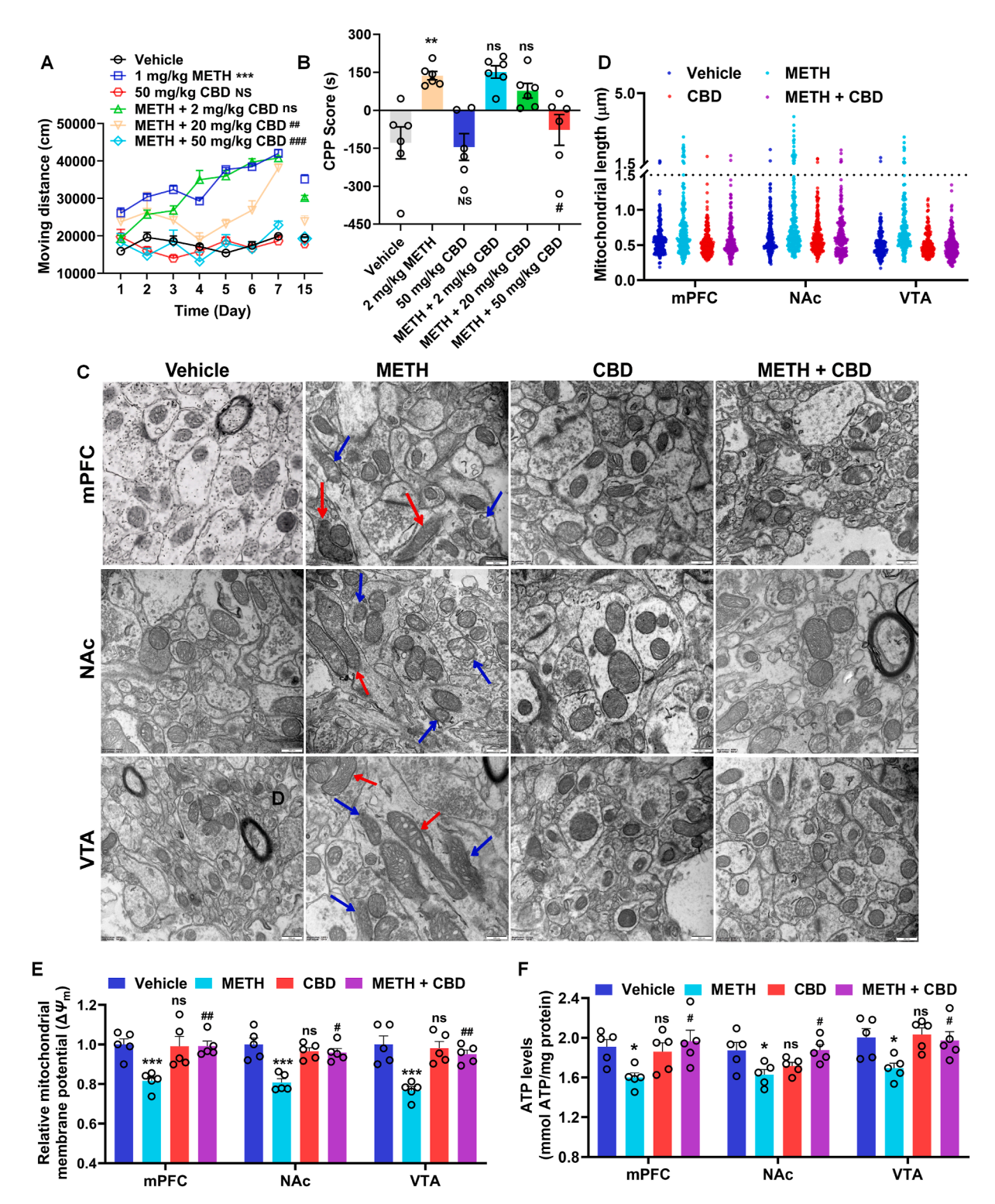


Figure 1 Cannabidiol (CBD) attenuates methamphetamine (METH)-induced addiction behaviors and reverses mitochondrial damage. (A) The effect of CBD on METH-induced behavioral sensitization (n = 5). (B) The effect of CBD on METH-induced conditioned place preference (CPP) (n = 6). (C-F) Mice were subjected to daily administrations of METH (2 mg/kg), CBD (50 mg/kg), or a combination of METH (2 mg/kg) + CBD (50 mg/kg) over a period of 14 days. (C) Representative transmission electron microscopy images illustrating the mitochondria in the medial prefrontal cortex (mPFC), nucleus accumbens (NAc), and ventral tegmental area (VTA) of mice across different treatment groups: vehicle group, METH group, CBD group, and METH + CBD group. Blue arrows: mitochondria with disrupted membrane and cristae structure; red arrows: swollen mitochondria. The scale bar corresponds to 500 nm (n = 6). (D) Effects of METH and CBD on mitochondrial length. No fewer than 200 mitochondria sourced from 6 distinct mice were analyzed for each group. (E, F) The effect of CBD on METH-induced decline of relative mitochondrial membrane potential ($\Delta\Psi$ m) (E) and adenosine triphosphate (ATP) (F) in the VTA of mice (n = 5). Data are expressed as

Chronic METH exposure led to damage of the inner mitochondrial membrane and a loss of cristae, and these METH-induced changes in mitochondrial morphology were effectively reversed by CBD (Fig. 1C). Similarly, CBD significantly reduced the number of swollen mitochondria (mitochondrial length>1.5 μm) induced by METH (Fig. 1D). Fresh mitochondria were isolated from the mPFC, NAc, and VTA, and the relative membrane potential $(\Delta\Psi_m)$ was measured. METH treatment resulted in the reduction of $\Delta\Psi_m$, and CBD treatment effectively inhibited the METH-induced $\Delta\Psi_m$ reduction (Fig. 1E). This mitochondrial damage impaired the ability of mitochondria to produce ATP efficiently, and CBD successfully counteracted the decrease in ATP caused by METH (Fig. 1F). These findings demonstrate that CBD prevents METH-induced mitochondrial damage and reverses METH-induced reduction in ATP.

3.2. Target fishing and the verification of ATP5A1 as a direct target for CBD

To identify the molecular target responsible for CBD's ability to prevent METH-induced mitochondrial damage, the photoaffinity CBD probe CP1 was synthesized (Supporting Information Scheme S1). This probe contains both a photoreactive benzophenone moiety and a terminal alkynyl group within the same molecule. The bioequivalence of CP1 relative to CBD was evaluated via a CPP assay. Although CP1 showed slightly attenuated efficacy compared to CBD in reducing METH-induced CPP, it retained substantial therapeutic effects and displayed comparable bioequivalence (Supporting Information Fig. S2). The workflow diagram for protein target identification was shown in Fig. 2A. Cells were subjected to CP1 either by itself or in combination with CBD acting as a competitive binding agent. Upon exposure to 365 nm UV light, the benzophenone moiety of CP1 underwent photoactivation, forming covalent links with the target proteins. Following cell lysis, biotin was attached to CP1 via the coppercatalyzed click reaction, where biotin azide reacted with the alkynyl group in CP1. Subsequently, proteins captured by CP1 were isolated using streptavidin-coated magnetic beads. CP2 (Scheme S1), which lacks the CBD moiety, was used as a control probe. The pull-downed proteins were subsequently subjected to SDS-PAGE and analyzed by silver staining. The bands enriched by CP1 were competitively inhibited by CBD (Fig. 2B). The bands specifically captured by CP1 were cut for proteolysis into peptides, followed by proteomic analysis by LC-MS/MS. The proteins that were captured by CP1 are shown in Supporting Information Table S6.

The proteins were clustered by gene ontology analysis based on their cellular component (Fig. 2C). Among the captured proteins, ATP5A1, a subunit of ATP synthase (complex V), garnered significant attention due to its high database search scores (Table S6) and CBD's involvement in preventing mitochondria and ATP metabolic processes. Moreover, ATP5A1 has been reported to be associated with drug addiction 15. Therefore, ATP5A1 was selected for subsequent target verification. As shown in Fig. 2D, the binding of CP1 to ATP5A1 was competitively inhibited by CBD, which indicates the specific binding between CBD and ATP5A1. Furthermore, a CETSA was conducted to verify whether ATP5A1 served as the specific binding partner for

CBD. The results of the CETSA demonstrated that CBD binding had the effect of enhancing the thermal stability of ATP5A1, as evidenced by the alteration in its melting temperature (Fig. 2E). To quantitively characterize the interaction of CBD with ATP5A1, fluorescence titration of the purified ATP5A1 by CBD was performed (Fig. 2F). The binding of CBD resulted in the quenching of ATP5A1 intrinsic fluorescence. A dissociation constant of 4.9 \pm 1.2 μ mol/L was derived for CBD–ATP5A1 interaction (Fig. 2F). The enzymatic activity assay revealed that CBD enhanced ATP synthase activity, achieving an EC50 value of 2.8 \pm 1.0 μ mol/L (Fig. 2G). Collectively, these results strongly suggest that ATP5A1 serves as a direct molecular target of CBD.

3.3. D376 of ATP5A1 is a critical residue mediating CBD's inhibition of METH-induced ubiquitination and degradation of ATP5A1

To assess the effect of CBD on the expression of ATP5A1, the tissues corresponding to the mPFC, NAc and VTA regions were collected following daily administrations of either METH (2 mg/kg), CBD (50 mg/kg), or a combined treatment of METH (2 mg/kg) + CBD (50 mg/kg) for 14 days and subjected to ATP5A1 immunofluorescence staining (Fig. 3A, Supporting Information Figs. S3 and S4). Chronic METH treatment reduced ATP5A1 protein expression in the VTA and CBD ameliorated METH-induced reduction of ATP5A1 protein (Fig. 3A and B).

However, no such changes were observed in the NAc and mPFC brain regions (Figs. S3 and S4). ATP5A1 was co-labeled with the neuronal marker neuronal nuclei antigen (NeuN), the microglial marker ionized calcium binding adapter molecule 1 (IBA1), and the astrocyte marker glial fibrillary acidic protein (GFAP) in Supporting Information Figs. S5-S7. METH-induced reductions of ATP5A1 in the VTA region occurred across multiple cell types, including neurons, microglia, and astrocytes, and CBD treatment effectively inhibited these reductions (Supporting Information Fig. S8). Further Western blot analysis of ATP5A1 in the VTA independently confirmed that the VTA plays a critical role in mediating the effects of CBD on METH-induced alterations in mitochondrial function and ATP5A1 expression (Fig. 3C). In addition to ATP5A1, the ATP synthase subunits ATP5B and ATP5C1 were explored, that the three of them are closely associated to form the F1 subunit of ATP synthase. The administration of METH, CBD, or their combination had no discernible impact on the levels of ATP5B and ATP5C1 expression, whether assessed at the protein level (Fig. 3C) or the mRNA level (Supporting Information Fig. S9). Subsequently, the ubiquitination of ATP5A1 was measured. Chronic METH treatment induced the excessive ubiquitination of ATP5A1, therefore resulting in the reduction of ATP5A1 protein (Fig. 3D). CBD was found to inhibit METH-induced ubiquitination of ATP5A1, thus preventing METH-induced reduction of ATP5A1 protein (Fig. 3D).

To further explore the consequences of the increased ATP5A1 levels on the assembly of ATP synthase, the VTA homogenates were subjected to immunoprecipitation with ATP5A1 antibody and immuno-detection by ATP synthase subunit beta (ATP5B) and ATP synthase subunit gamma (ATP5C1) antibodies (Fig. 3E).

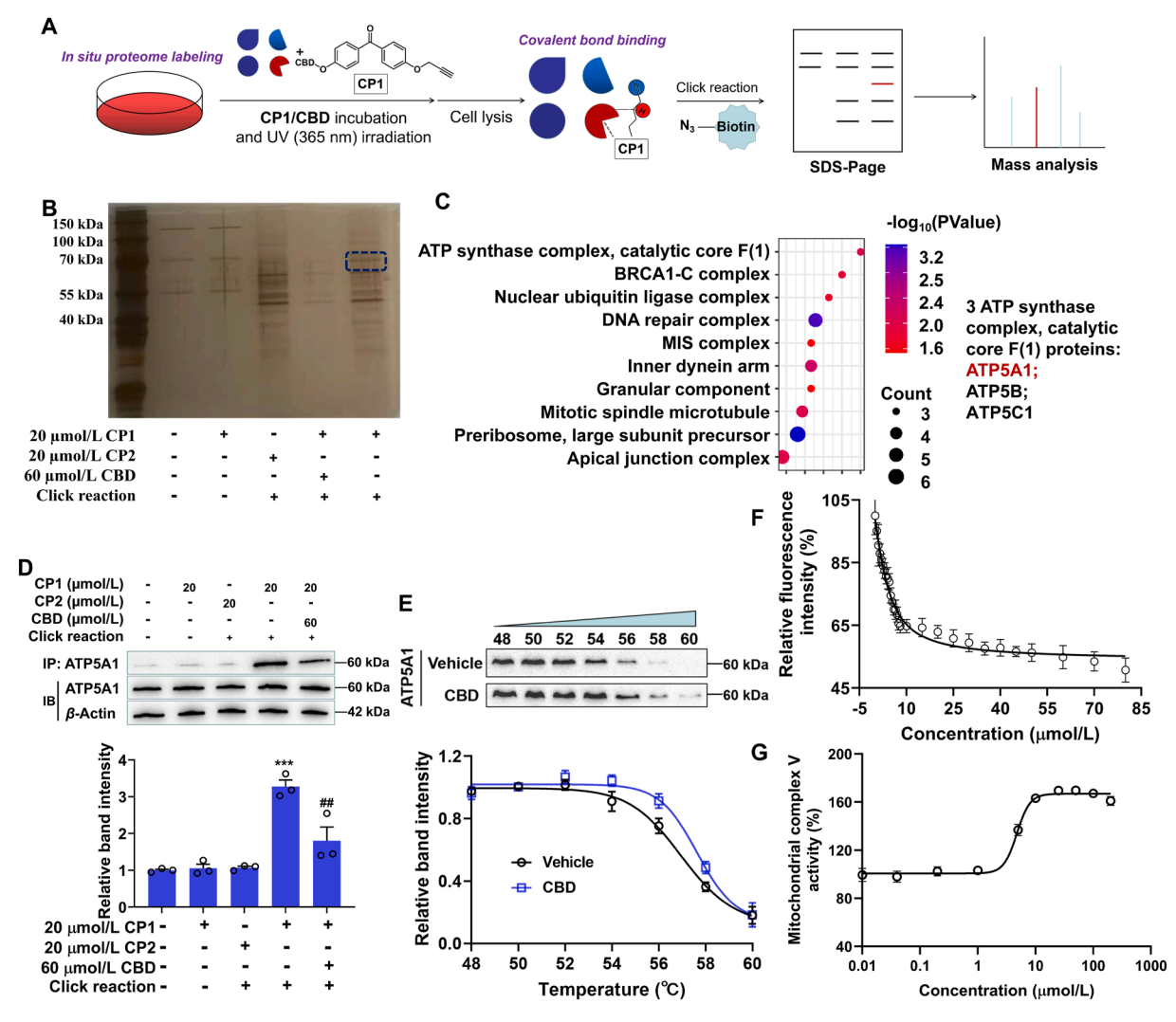


Figure 2 ATP synthase F1 subunit alpha (ATP5A1) was the target of CBD. (A) Schematic illustration for the pull-down experiment of the CBD probe. (B) Silver staining SDS-PAGE of enriched proteins by pull-down probes. (C) Clustering of the proteins from the CBD pull-down assay on the basis of the cellular component. (D) Pull-down/Western blotting for target validation of ATP5A1 with CBD pull-down probes. (E) CETSA for characterizing the interaction of endogenous ATP5A1 with CBD. (F) Fluorescence titration curve of ATP5A1 with CBD. $K_D = 4.9 \pm 1.2 \mu \text{mol/L}$ was obtained. (G) CBD exhibited enhancement of ATP synthetase activity, with an EC₅₀ value of $2.8 \pm 1.0 \mu \text{mol/L}$. Data are expressed as mean \pm SEM of three independent experiments and were analyzed by one-way ANOVA. ***P < 0.001 versus the vehicle group; *#P < 0.01 versus the group with CP1 probe and click reaction.

ATP5B and ATP5C1 were co-immunoprecipitated with ATP5A1. Chronic METH treatment led to a decrease in the recruitment of ATP5C1 with ATP5A1, yet it did not affect the association between ATP5B and ATP5A1. Conversely, CBD effectively reversed the decline in ATP5C1 recruitment caused by METH, suggesting that CBD may have the capacity to enhance ATP synthase levels, CBD reversed METH-induced decline of mitochondrial complexes as revealed by blue native PAGE (BN-PAGE) analysis (Fig. 3F). The band, which was primarily comprised of subunits of ATP synthase (Supporting Information Table S7), was verified as Complex V. Further immunoblotting for BN-PAGE by ATP5A1 antibody revealed that CBD attenuated METH-induced reduction in both monomeric and dimeric forms of ATP synthases (Fig. 3G). In summary, these findings collectively show that CBD mitigates the ubiquitination of ATP5A1 induced by METH and counteracts the METH-induced decrease in ATP5A1 protein, thereby facilitating the assembly of ATP synthase.

To identify the critical amino acid residues mediating CBD interaction with ATP5A1, in silico docking was conducted to pinpoint the binding location within the box, which contained the ATP5A1, ATP5B, and ATP5C1 subunits of ATP synthase (Supporting Information Fig. S10). The results indicated that CBD bound at the interface between ATP5A1, ATP5B, and ATP5C1 subunits. Within this interface, the hydroxyl groups of CBD established hydrogen bonds with D376 in ATP5A1 and O280 in ATP5C1 (Fig. 4A and B), which is consistent with the observation that ATP synthase subunit ATP5C1 was found in the proteins captured by CP1 probe activity-based protein profiling approach. The wild-type ATP5A1 and the ATP5A1 D376A mutant was expressed and purified, followed by a protein thermal shift assay. CBD significantly enhanced the thermal stability of wild-type ATP5A1 as reflected by the shift of its melting temperature $(T_{\rm m})$ with $\Delta T_{\rm m}$ of 4.7 \pm 0.4 °C. However, CBD did not affect the thermal stability of the mutant protein after incubation with

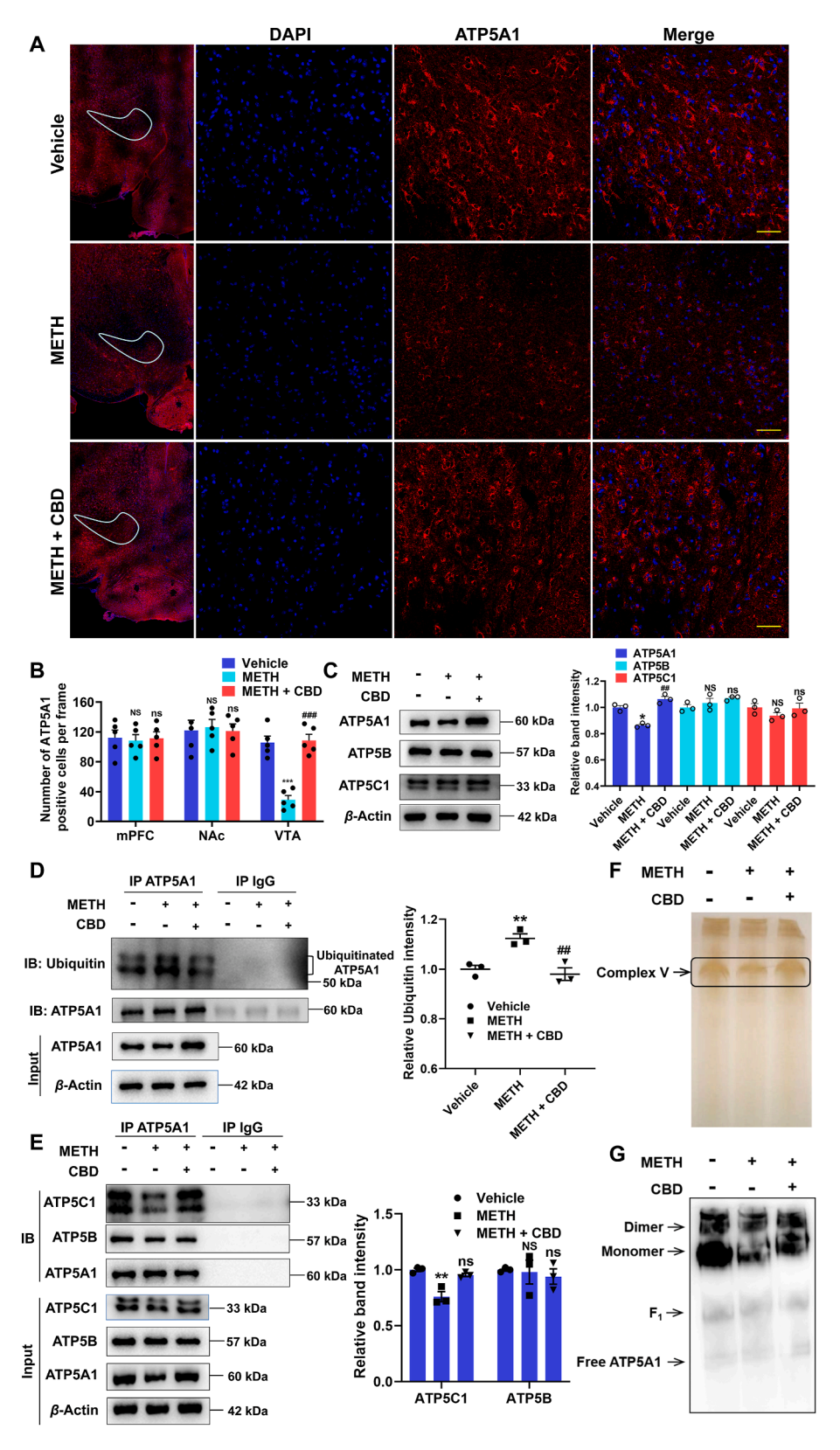
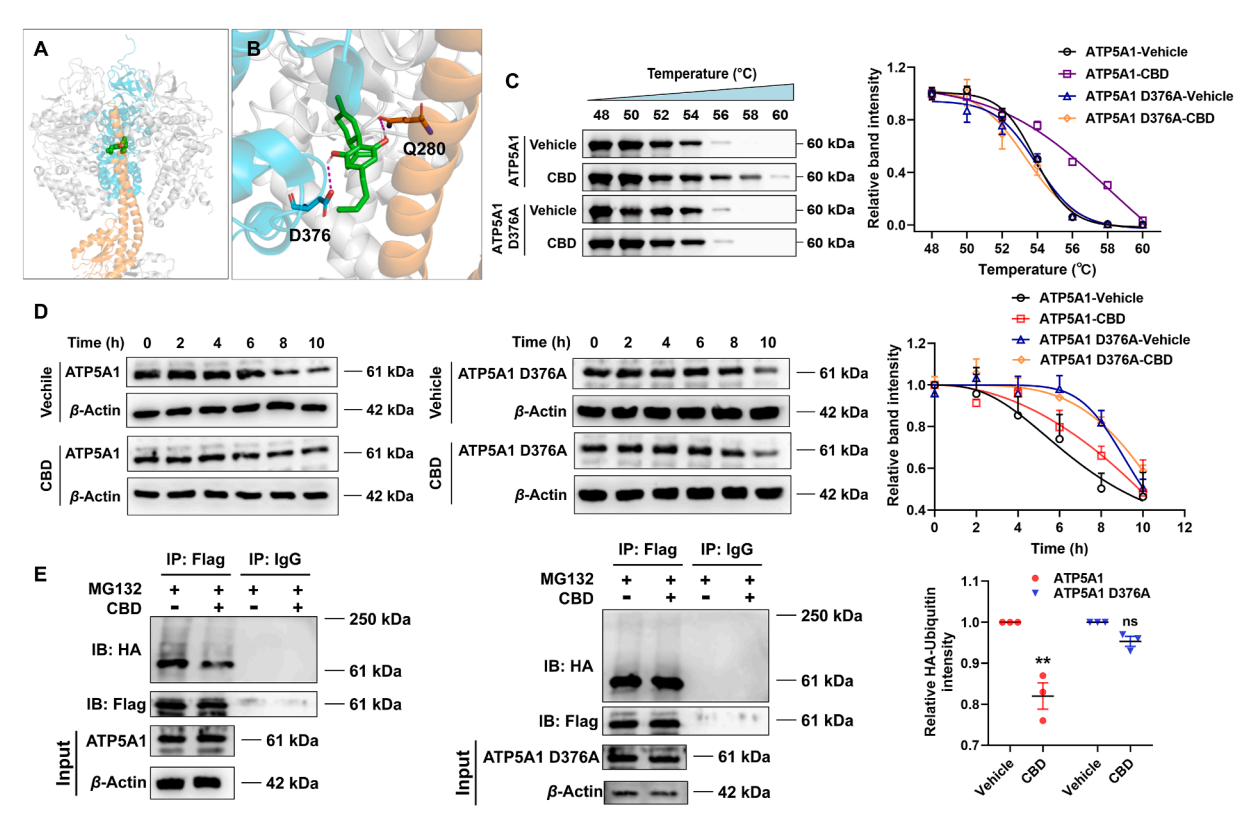


Figure 3 CBD restores METH-induced ATP5A1 decline and promotes ATP synthase assembly by inhibiting ATP5A1 ubiquitination. (A–H). Mice were subjected to daily administrations of METH (2 mg/kg), CBD (50 mg/kg), or a combination of METH (2 mg/kg) + CBD (50 mg/kg) over a period of 14 days. (A) Representative immunofluorescence images of ATP5A1 in the VTA (scale: 40 μ m). (B) The quantification of the expression of ATP5A1 in the mPFC, NAc, and VTA regions shown in panel (A) and Supporting Information Figs. S and S4 (n = 5). (C) ATP5A1, ATP5B, and ATP5C1 protein levels in the VTA region were detected by immunoblotting (n = 3). (D) Following co-immunoprecipitation by anti-ATP5A1 antibody, the ubiquitination of ATP5A1 in the VTA region was also measured (n = 3). Furthermore, the interaction between ATP5A1,



ATP5A1 D376A (Fig. 4C). Similarly, CBD failed to suppress the intrinsic fluorescence of ATP5A1 D376A, indicating that the D376 of ATP5A1 is a critical residue for CBD binding (Supporting Information Fig. S11). To further explore the influence of the D376 in ATP5A1 on the regulation of its ubiquitination level by CBD, Flag-tagged ATP5A1 or ATP5A1 D376A was co-transfected with HA-ubiquitin into HEK293T cells. The synthesis of ATP5A1 was blocked with 50 µg/mL CHX, and the cells were then treated with 10 µmol/L CBD. The effect of CBD on the degradation rate of ATP5A1 was examined via immunoblotting. After CHX treatment, the level of wild-type ATP5A1 decreased by approximately 50% within 8 h, while the ATP5A1 content remained at about 70% after CBD treatment (Fig. 4D). Thus, CBD significantly extended the half-life of ATP5A1 from 6.6 \pm 1.4 to 8.1 ± 1.7 h. However, CBD failed to inhibit the degradation of ATP5A1 D376A. Subsequently, 10 µmol/L MG132 was used to inhibit proteasomal degradation in HEK293T cells to investigate the mechanism underlying CBD-mediated inhibition of ATP5A1 degradation. After 8 h of CBD treatment, wild-type ATP5A1 ubiquitination was significantly reduced, whereas that of ATP5A1 D376A showed no significant change (Fig. 4E). Collectively, these results suggest that D376 of ATP5A1 is a key residue through which CBD modulates METH-induced ubiquitination and degradation in the VTA region.

3.4. CBD inhibits METH-induced behavioral addiction via ATP5A1-ATP-ADO-A1R signaling pathway

Beyond its role as an energy molecule, ATP has gained recognition as a signaling molecule in recent years 34,35 . The elevated ATP was released extracellularly and transformed into adenosine, which activates the A_1R . This adenosine- A_1R interaction leads to the dampening of neuronal excitability 36 , offering a promising avenue for mitigating METH-induced addictive behaviors. The therapeutic effects of CBD in reducing METH-induced behavioral sensitization (Fig. 5A and B) and CPP (Fig. 5C) were diminished

ATP5B, and ATP5C1 in the VTA region was measured by co-immunoprecipitation (n=3) (E). Following the isolation of mitochondria from the VTA region, blue native PAGE (BN-PAGE, F) was performed to quantify the composition of the mitochondrial respiratory chain complexes (n=3). After BN-PAGE, the mitochondrial lysates were also subjected to ATP5A1 immunoblotting (n=3, G). Data are expressed as mean \pm SEM and were analyzed by one-way ANOVA. ^{NS}P>0.05, **P<0.05, **P<0.05, ***P<0.05, ***P<0.01, ***P<0.001 versus the vehicle group; P>0.05, ***P<0.01, ***P<0.001 versus the METH group.

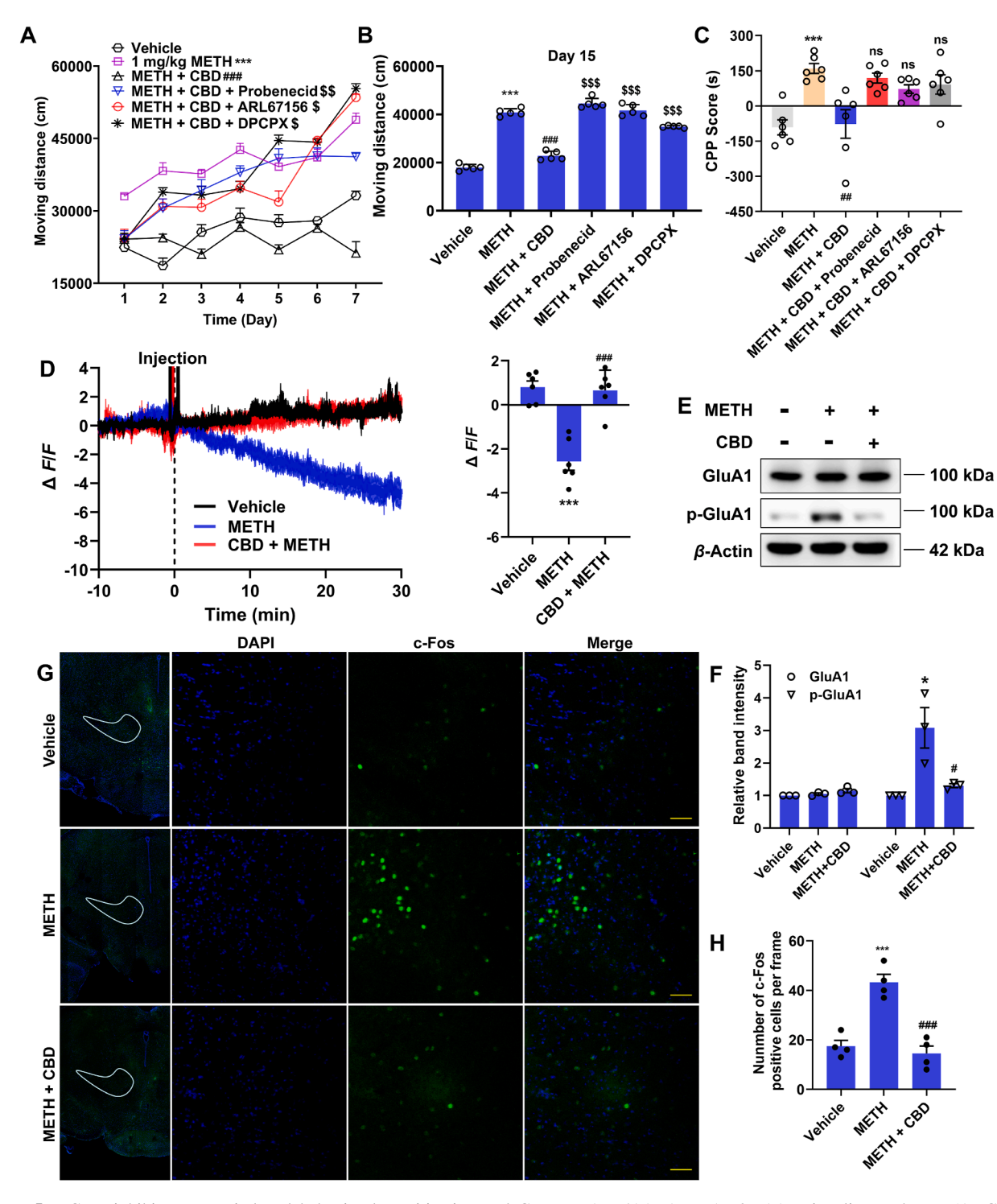


Figure 5 CBD inhibits METH-induced behavioral sensitization and CPP via ATP5A1-ATP-ADO-A1R signaling pathway. (A-C) The effects of pannexin 1 (PANX1) antagonist (Probenecid, 50 mg/kg, i.p.), ectonucleoside triphosphate diphosphohydrolase-1 (CD39) antagonist (ARL67156, 0.1 mg/kg, i.p.) and adenosine A1R antagonist (DPCPX, 1 mg/kg, i.p.) on the therapeutic effects of CBD (50 mg/kg) in METH (2 mg/kg)-induced behavioral sensitization (A, B, n = 5) and CPP (C, n = 6). (D) Adenosine triphosphate (ATP) $\Delta F/F$ ratios measured in the VTA region of mice following 7-day administration of 2 mg/kg METH and 50 mg/kg CBD (n = 6). (E, F) Ionotropic glutamate receptors (GluA1) and p-GluA1 protein levels in the VTA region were detected by immunoblotting (n = 3). (G, H) Fos proto-oncogene (c-Fos) expression in the VTA brain region (n = 4). Mice were subjected to daily administrations of METH (2 mg/kg), CBD (50 mg/kg), or a combination of METH (2 mg/kg) + CBD (50 mg/kg) over a period of 14 days. 90 min after the final administration, the mice were sacrificed to assess c-Fos expression. The scale represents 40 μ m. Data are expressed as mean \pm SEM. Data of Fig. 5A were analyzed by paired t-test. Data of Fig. 5B-H were analyzed by one-way ANOVA. *P < 0.05, ***P < 0.001 versus the vehicle group; *P < 0.05, **P < 0.05, ***P < 0.01, ****P < 0.01 versus the METH group; *P < 0.05, **P < 0.05, ***P < 0.01 versus the METH CBD group.

when the ATP efflux channel PANX1 was pharmacologically inhibited with probenecid. This suggests that CBD's ability to prevent METH-induced behavioral addiction must involve the release of ATP into the extracellular space to produce its functional effects. Ectonucleoside triphosphate diphosphohydrolase 1 (CD39), the rate-limiting enzyme involved in transforming ATP into adenosine monophosphate (AMP), functions as an enzyme facilitating the conversion of ATP into AMP, which is subsequently metabolized into ADO by cluster of differentiation 73 (CD73)^{34,37}. ARL67156, a CD39 inhibitor, was used to block the hydrolysis of ATP and the formation of adenosine. The administration of ARL67156 or A1R antagonist DPCPX attenuated the therapeutic effects of CBD on METH-induced behavioral sensitization (Fig. 5A and B) and CPP (Fig. 5C).

To investigate the effects of CBD administration on extracellular ATP levels, the AAV9-EF1α-ATP viral vector was stereotaxically expressed in the VTA of mice (Supporting Information Fig. S12). Following 7 consecutive days of METH and CBD administration, extracellular ATP levels were monitored before and after METH challenge. Acute METH challenge induced a rapid, time-dependent decrease in extracellular ATP levels within 30 min (Fig. 5D). Notably, CBD treatment fully restored ATP concentrations to baseline levels comparable to vehicle controls. Extracellular ATP is metabolized to ADO, which directly activates Gi-coupled A1R. This activation suppresses phosphorylation of the ionotropic glutamate receptors (GluA1), thereby inhibiting dopamine D1 receptor activation and subsequent neuronal excitation^{38,39}. Immunoblotting analysis revealed that CBD treatment significantly attenuated A1R activation and markedly reduced METH-induced phosphorylation of the GluA1 (Fig. 5E and F). Furthermore, CBD treatment significantly inhibited the METH-induced increase in the immediate early gene protein, fos proto-oncogene (c-Fos) in the VTA brain region (Fig. 5G and H). These findings suggest that the interaction between adenosine and A1R plays a significant role in the context of METH addiction. By targeting ATP5A1, CBD regulates the ADO-A1R signaling pathway (Supporting Information Fig. S13), presenting a promising avenue for therapeutic intervention in METH addiction.

CBD promoted the assembly of ATP synthase via ATP5A1, improving mitochondrial function, and thereby activating the ADO-A1R signaling pathway. To directly verify whether ATP5A1 is the specific target of CBD in the treatment of METH addiction, Adeno Associated Virus 9 (AAV9)-based shRNA silencing was performed to investigate the therapeutic potential of ATP5A1 (Fig. 6A). The virus was mainly expressed in the VTA brain region (Fig. 6B). The expression of ATP5A1 in the VTA region exhibited a significant reduction two weeks after the administration of AAV9-shRNA targeting ATP5A1 (Fig. 6C, Supporting Information Fig. S14). There were no significant changes in caspase-3 and cleaved caspase-3 levels after shATP5A1 virus injection, indicating that ATP5A1 interference did not induce apoptosis (Fig. 6C). METH treatment elicited comparable behavioral sensitization (Fig. 6D and E) and CPP (Fig. 6F) responses in both the ATP5A1 shRNA-treated and mock shRNA-treated groups. CBD treatment effectively suppressed METH-induced locomotor sensitization (Fig. 6D and E) and CPP (Fig. 6F) in mock shRNA-treated mice. The RNA interference targeting ATP5A1 in the VTA region led to the reversal of CBD's therapeutic effectiveness in mitigating METH-induced behavioral

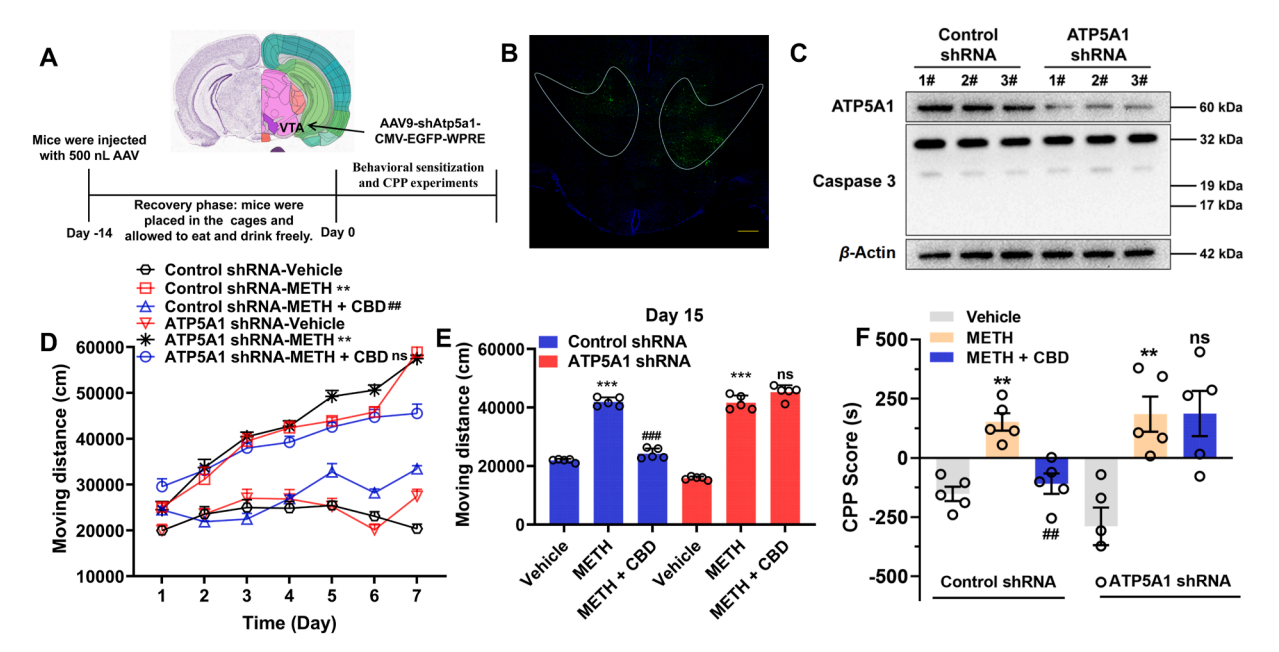


Figure 6 The therapeutic effect of CBD on METH addiction is hindered by ATP5A1 RNA interference. (A) Schematic illustration outlining the ATP5A1 RNA interference process in the VTA of mice (Quoted from Allen Brain Atlas). (B) EGFP-labeled fluorescent images of the viral injection site (scale: 300 µm). (C) ATP5A1 interference efficiency was detected by immunoblotting (n = 3). (D–F) Behavioral sensitization (D, E) and CPP. (F) assessments conducted in mock shRNA or ATP5A1 shRNA treated mice (n = 5). The doses of METH used for behavioral sensitization and CPP assays were 1 and 2 mg/kg, respectively. The dose of CBD was 50 mg/kg. Data are expressed as mean \pm SEM. Data of Fig. 6D were analyzed by paired t-test. Data of Fig. 6E and F were analyzed by one-way ANOVA. **P < 0.01, ***P < 0.001 versus the vehicle group; n P > 0.05, **P < 0.01, ***P < 0.001 versus the METH-treated group.

sensitization (Fig. 6D and E) and CPP (Fig. 6F). Collectively, these findings suggest that ATP5A1 serves as a target for CBD to suppress METH-induced addictive behaviors *via* modulation of the ADO—A1R signaling pathway.

4. Discussion

METH is a powerful CNS stimulant known for its addictive potential. Mitochondria, the cell's energy factories that produce the majority of ATP, are herein recognized as being susceptible to the harmful effects of METH. Chronic METH use inhibits dopamine transporters, leading to increased extracellular dopamine levels⁴⁰. The elevated dopamine undergoes oxidation, producing reactive oxygen species, which impair mitochondrial ATP production and function, exacerbating neurotoxicity and contributing to neurodegenerative diseases⁴¹. Chronic METH exposure led to damage of the inner mitochondrial membrane and a loss of cristae, resulting in a lowered mitochondrial membrane potential and decreased ATP generation. CBD is one of the most extensively investigated non-psychotrophic cannabinoids derived from the Cannabis sativa plant⁴². Recent studies indicate that CBD interacts with mitochondria, potentially safeguarding their function in situations of stress or injury 43,44. Since mitochondrial dysfunction contributes to the neural adaptations and behavioral changes seen in substance abuse disorders^{45,46}, CBD holds therapeutic promise for METH addiction. Indeed, CBD alleviated METH-induced locomotor sensitization and CPP. CBD was found to protect against the mitochondrial harm caused by METH and reversed METH-induced reduction in ATP. With regard to the potential toxic effects of METH, our behavioral assessments indicate that the tested doses reliably induce addiction-relevant phenotypes without eliciting overt signs of neurotoxicity. However, we acknowledge that distinguishing mitochondrial alterations that are specifically associated with addiction-related neuroadaptations from those resulting from low-grade cellular stress remains a complex challenge. Given the dual role of mitochondria in both cellular energy production and stress signaling, some of the observed mitochondrial changes may reflect early subtoxic stress responses rather than frank neurotoxicity. Therefore, future studies incorporating a broader panel of mitochondrial and cellular toxicity markers will be critical for delineating the threshold between adaptive neuroplasticity involved in addiction and the onset of mitochondrial dysfunction that could compromise neuronal integrity.

It has been suggested that the cannabinoid receptor type 1 (CB1) and cannabinoid receptor type 2 (CB2) play a role in substance use disorders^{47,48}. Yet, CBD shows a poor binding affinity to CB1 and CB2 receptors⁴⁹. Nevertheless, the molecular target and the underlying mechanism through which CBD treats METH addiction remain largely unexplored. Herein, ATP5A1, a subunit of ATP synthase, was identified as a target for CBD by the activity-based protein profiling approach. This finding was further corroborated through a combination of wet-lab techniques and in silico biophysical analyses. CBD was predicted to bind at the interface between ATP5A1, ATP5B, and ATP5C1 subunits, therefore promoting the assembly of ATP synthetase and reversing METH-induced ATP reduction. CBD inhibited the ubiquitination of ATP5A1 induced by METH and prevented the METH-caused decrease in ATP5A1 protein level. The upregulation of ATP5A1 increases the availability of core subunits essential for ATP synthase assembly, thereby enhancing mitochondrial ATP production and restoring energy balance disrupted by METH exposure. However, it is important to acknowledge that small molecules like CBD often display promiscuity characterized by interactions with other molecular targets. CBD is known to interact with several molecular targets, including transient receptor potential vanilloid 1 (TRPV1)⁵⁰, voltage-gated sodium channel 1.7 (Nav1.7)⁵¹, G protein-coupled receptor 55 (GPR55)⁵², and peroxisome proliferator-activated receptor gamma (PPAR γ)⁵³. While the present study identifies ATP5A1 as a key mediator of CBD's protective effects against METH-induced mitochondrial dysfunction, the extent to which these additional targets contribute to CBD's therapeutic efficacy in METH addiction remains unclear. Elucidating their roles will require further mechanistic studies, which may uncover complementary or synergistic pathways involved in CBD's multifaceted actions.

Microglia and astrocytes are two key cell types involved in the secretion of extracellular ATP^{54,55}. The ATP discharged by these cells further regulates neurons^{56,57}, indicating potential effects in METH addiction. The elevated ATP is released into the extracellular space and metabolized into ADO, which then activates A1R⁵⁸. This adenosine—A1R interaction leads to the suppression of the release of glutamate⁵⁹ and dopamine⁶⁰, neurotransmitters often implicated in the reward and addiction pathways. Blocking the ATP efflux channel PANX1, inhibiting ATP hydrolysis with the CD39 inhibitor, and obstructing the A1R reduced CBD's effects against METH-induced behavioral sensitization and CPP. METH increases dopamine levels in the synaptic cleft by blocking dopamine transporters, leading to the activation of dopamine D1 receptors⁶¹. A1R negatively interacts with dopamine D1 receptors^{38,62}. Activation of A1R inhibits dopamine receptors, reducing dopamine release and neuronal activation⁵⁸. This study shows that CBD targets ATP5A1, leading to increased ATP production. The overproduction of ATP results in elevated extracellular adenosine levels and activation of the A1R signaling pathway. Therefore, it is not surprising that CBD treatment reduces cFos expression in the VTA, inhibits METH-induced neuronal activation, and consequently suppresses METH addiction. Additionally, RNA interference of ATP5A1 in the VTA diminished CBD's therapeutic efficacy against METH addiction. In sum, these data show that ATP5A1 is a target for CBD, countering METH addiction via the ADO-A1R signaling pathway.

While the present study focused on the global modulatory effects of CBD on ATP5A1 across neural populations, it is critical to recognize the cellular heterogeneity of the central nervous system. Neurons, microglia, and astrocytes not only fulfill distinct physiological roles but also exhibit divergent metabolic demands and regulatory mechanisms for mitochondrial function. Given the central role of neurons in addiction-related circuitry and the relatively high expression of ATP5A1 in neuronal populations, future investigations should employ cell-type-specific viral vectors (e.g., using neuron- or glia-specific promoters) to dissect the cellular origins of CBD's effects. Such an approach will be essential to clarify the contribution of individual cell types to CBD's anti-addictive mechanisms, enabling a more nuanced understanding of the circuit-level dynamics through which mitochondrial modulation translates into behavioral outcomes.

Beyond addiction, numerous neurological and psychiatric disorders, including Alzheimer's disease⁶³, Parkinson's disease⁶⁴, and depression⁶⁵ are characterized by mitochondrial dysfunction or impaired energy metabolism, highlighting the broader therapeutic potential of CBD in these conditions. Despite its promising

effects, CBD's clinical application is hindered by poor bioavailability, which necessitates high dosing and increases the risk of adverse effects, thereby limiting its therapeutic window. Structural optimization of CBD offers a compelling approach to overcome these limitations by enhancing its potency and target specificity, ultimately improving both efficacy and safety in clinical settings.

5. Conclusions

This study verifies that ATP5A1 directly binds with CBD both *in vitro* and *in vivo*, counteracting METH-triggered ATP5A1 ubiquitination and enhancing the assembly of ATP synthase, thereby preventing METH-induced mitochondrial damage. Additionally, CBD inhibits METH-induced addictive behaviors through the ADO-A1R signaling pathway. The results indicate that CBD alleviates methamphetamine addiction by targeting ATP5A1. Besides METH, CBD has shown potential therapeutic effects on addiction to opioids ¹⁸ and THC ⁶⁶. This implies that CBD has therapeutic potential for various forms of substance abuse. Consequently, ATP5A1 may serve as a target in the treatment of polysubstance use disorders, which warrants further exploration.

Acknowledgments

This work was supported by the National Natural Science Foundation of China (22207105; 22277118; T2241028), the STI2030-Major Projects (2021ZD0203000 (2021ZD0203003), China), Talent Introduction Project of Shandong First Medical University funds under Grant YS23-0000349, the Science and Technology Innovation Program of the Chinese Academy of Agricultural Sciences (No. CAAS-ASTIP-2021-ISAPS, China), the Key Science and Technology Project of Jilin Province (20200504001YY, China), Science and Technology Development Plan Project of Jilin Province (20220204045GH, China), International Partnership Program of the Chinese Academy of (029GJHZ2024057GC, China), Open Research Fund of the State Key Laboratory of Brain Machine Intelligence, Zhejiang University (BMI2400014, China), and National Natural Science Foundation of Hunan Province (2025JJ70246, China). We are grateful to Can Peng and Xixia Li for helping with electron microscopy sample preparation and taking TEM images at the Center for Biological Imaging (CBI), Institute of Biophysics, Chinese Academy of Science. We would like to thank the Key Laboratory of Molecular Epigenetics, Ministry of Education, and the Institute of Genetics and Cytology, Northeast Normal University for providing access to laser confocal microscope.

Author contributions

Xiaohui Wang designed the research; Sha Jin, Cong Lin, Peipei Li, Xue Wang, Cong Zhang and Xuenan Wang performed the experiments, Sha Jin, Peipei Li, Cong Lin, Xuenan Wang, Xue Wang, and Xiaohui Wang analyzed the data; Sha Jin, Cong Lin and Xiaohui Wang wrote the manuscript; Haohong Li, Yinghua Peng, Yuyuan Lu and Xiaohui Wang edited the manuscript. All authors read and approved the final manuscript.

Conflicts of interest

The authors declare no conflicts of interest.

Appendix A. Supporting information

Supporting information to this article can be found online at https://doi.org/10.1016/j.apsb.2025.08.011.

References

- Courtney KE, Ray LA. Methamphetamine: an update on epidemiology, pharmacology, clinical phenomenology, and treatment literature. *Drug Alcohol Depend* 2014;143:11—21.
- McCabe SE, Schulenberg JE, Wilens TE, Schepis TS, McCabe VV, Veliz PT. Cocaine or methamphetamine use during young adulthood following stimulant use for attention-deficit/hyperactivity disorder during adolescence. *JAMA Netw Open* 2023;6:e2322650.
- Friedman J, Beletsky L, Schriger DL. Methamphetamine overdose deaths in the US by sex and race and ethnicity. *JAMA Psychiat* 2021; 78:564-7
- Hedges DM, Obray JD, Yorgason JT, Jang EY, Weerasekara VK, Uys JD, et al. Methamphetamine induces dopamine release in the nucleus accumbens through a sigma receptor-mediated pathway. *Neuropsychopharmacology* 2017;43:1405–14.
- Shah A, Kumar S, Simon SD, Singh DP, Kumar A. HIV gp120 and methamphetamine-mediated oxidative stress induces astrocyte apoptosis via cytochrome P450 2E1. Cell Death Dis 2013;4:e850.
- Abdullah CS, Aishwarya R, Alam S, Morshed M, Remex NS, Nitu S, et al. Methamphetamine induces cardiomyopathy by sigmal inhibition-dependent impairment of mitochondrial dynamics and function. *Commun Biol* 2020;3:628.
- Hossain Khan F, Sen T, Maiti AK, Jana S, Chatterjee U, Chakrabarti S. Inhibition of rat brain mitochondrial electron transport chain activity by dopamine oxidation products during extended *in vitro* incubation: implications for Parkinson's disease. *Biochim Biophys Acta* 2005;1741: 65-74.
- Jana S, Sinha M, Chanda D, Roy T, Banerjee K, Munshi S, et al. Mitochondrial dysfunction mediated by quinone oxidation products of dopamine: implications in dopamine cytotoxicity and pathogenesis of Parkinson's disease. *Biochim Biophys Acta Mol Basis Dis* 2011;**1812**: 663-73
- Wang L, Wei QF, Xu R, Chen YX, Li S, Bu Q, et al. Cardiolipin and OPA1 team up for methamphetamine-induced locomotor activity by promoting neuronal mitochondrial fusion in the nucleus accumbens of mice. ACS Chem Neurosci 2023;14:1585—601.
- Yan PJ, Ren ZX, Shi ZF, Wan CL, Han CJ, Zhu LS, et al. Dysregulation of iron homeostasis and methamphetamine reward behaviors in Clk1-deficient mice. *Acta Pharmacol Sin* 2022;43:1686–98.
- Corkrum M, Covelo A, Lines J, Bellocchio L, Pisansky M, Loke K, et al. Dopamine-evoked synaptic regulation in the nucleus accumbens requires astrocyte activity. *Neuron* 2020;105:1036–47.
- Fields RD, Burnstock G. Purinergic signalling in neuron—glia interactions. Nat Rev Neurosci 2006;7:423—36.
- Peng WL, Wu ZF, Song K, Zhang SY, Li YL, Xu M. Regulation of sleep homeostasis mediator adenosine by basal forebrain glutamatergic neurons. *Science* 2020;369:eabb0556.
- Sun XD, Li L, Liu F, Huang ZH, Bean JC, Jiao HF, et al. Lrp4 in astrocytes modulates glutamatergic transmission. *Nat Neurosci* 2016; 19:1010–8.
- del Castillo C, Morales L, Alguacil LF, Salas E, Garrido E, Alonso E, et al. Proteomic analysis of the nucleus accumbens of rats with different vulnerability to cocaine addiction. *Neuropharmacology* 2009;57:41–8.
- Pérez-Ortiz JM, Galiana-Simal A, Salas E, González-Martín C, García-Rojo M, Alguacil LF. A high-fat diet combined with food deprivation increases food seeking and the expression of candidate biomarkers of addiction. *Addict Biol* 2017;22:1002—9.
- Ledesma JC, Manzanedo C, Aguilar MA. Cannabidiol prevents several of the behavioral alterations related to cocaine addiction in mice. Prog Neuropsychopharmacol Biol Psychiatry 2021;111:110390.

- Ren YH, Whittard J, Higuera-Matas A, Morris CV, Hurd YL. Cannabidiol, a nonpsychotropic component of cannabis, inhibits cueinduced heroin seeking and normalizes discrete mesolimbic neuronal disturbances. J Neurosci 2009;29:14764—9.
- Umpierrez LS, Costa PA, Michelutti EA, Baracz SJ, Sauer M, Turner AJ, et al. Cannabidiol but not cannabidiolic acid reduces behavioural sensitisation to methamphetamine in rats, at pharmacologically effective doses. *Psychopharmacology* 2022;239:1593-603.
- 20. Zhang D, Zeng X, Shen B, Li Y, Huang J, Leung CK, et al. Cannabidiol attenuates methamphetamine-induced conditioned place preference via the sigma1R/AKT/GSK-3β/CREB signaling pathway in rats. Toxicol Res 2020;9:202–11.
- Xiaohui L, Jingyuan Z, Huijiao L, Wenqiang M, Leo Y, Xin T, et al. Cannabidiol attenuates pulmonary arterial hypertension by improving vascular smooth muscle cells mitochondrial function. *Theranostics* 2021:11:5267-78.
- Yang S, Du Y, Zhao X, Tang Q, Su W, Hu Y, et al. Cannabidiol enhances microglial beta-amyloid peptide phagocytosis and clearance via vanilloid family type 2 channel activation. Int J Mol Sci 2022;23:5367.
- Ibork H, Idrissi SE, Zulu SS, Miller R, Hajji L, Morgan AM, et al. Effect of cannabidiol in LPS-induced toxicity in astrocytes: possible role for cannabinoid type-1 receptors. *Neurotox Res* 2023;41:615–26.
- 24. Moriguchi S, Nishi M, Sasaki Y, Takeshima H, Fukunaga K. Aberrant behavioral sensitization by methamphetamine in junctophilin-deficient mice. *Mol Neurobiol* 2014;**51**:533–42.
- Genmeng Y, Liu L, Ruilin Z, Juan L, Chi-Kwan L, Jian H, et al. Cannabidiol attenuates methamphetamine-induced conditioned place preference *via* the Sigma1R/AKT/GSK-3β/CREB signaling pathway in rats. *Toxicol Res* 2020;9:202–11.
- Wang X, Lin C, Jin S, Wang YB, Peng YH, Wang XH. Cannabidiol alleviates neuroinflammation and attenuates neuropathic pain *via* targeting FKBP5. *Brain Behav Immun* 2023;111:365–75.
- Watt IN, Montgomery MG, Runswick MJ, Leslie AGW, Walker JE. Bioenergetic cost of making an adenosine triphosphate molecule in animal mitochondria. *Proc Natl Acad Sci USA* 2010;107:16823—7.
- Madhavi SG, Adzhigirey M, Day T, Annabhimoju R, Sherman W. Protein and ligand preparation: parameters, protocols, and influence on virtual screening enrichments. *J Comput Aided Mol Des* 2013;27: 221–34.
- Eberhardt J, Santos-Martins D, Tillack AF, Forli S. AutoDock vina 1.2.0: new docking methods, expanded force field, and python bindings. *J Chem Inf Model* 2021;61:3891–8.
- Trott O, Olson AJ. AutoDock Vina: improving the speed and accuracy of docking with a new scoring function, efficient optimization, and multithreading. J Comput Chem 2009;31:455—61.
- 31. Lancet T. Opioids and methamphetamine: a tale of two crises. *Lancet* 2018;**391**:713.
- 32. Mohammadi M, Eskandari K, Azizbeigi R, Haghparast A. The inhibitory effect of cannabidiol on the rewarding properties of methamphetamine in part mediates by interacting with the hippocampal D1-like dopamine receptors. *Prog Neuropsychopharmacol Biol Psychiatry* 2023;126:110778.
- Cruickshank CC, Dyer KR. A review of the clinical pharmacology of methamphetamine. *Addiction* 2009;104:1085—99.
- Dwyer KM, Kishore BK, Robson SC. Conversion of extracellular ATP into adenosine: a master switch in renal health and disease. *Nat Rev Nephrol* 2020;16:509–24.
- 35. Huang Z, Xie N, Illes P, Di Virgilio F, Ulrich H, Semyanov A, et al. From purines to purinergic signalling: molecular functions and human diseases. *Signal Transduct Target Ther* 2021;6:162.
- **36.** Dunwiddie TV, Masino SA. The role and regulation of adenosine in the central nervous system. *Annu Rev Neurosci* 2001;**24**:31–55.
- Lanser AJ, Rezende RM, Rubino S, Lorello PJ, Donnelly DJ, Xu HX, et al. Disruption of the ATP/adenosine balance in CD39 mice is associated with handling-induced seizures. *Immunology* 2017;152:
- 38. Yabuuchi K, Kuroiwa M, Shuto T, Sotogaku N, Snyder GL, Higashi H, et al. Role of adenosine A1 receptors in the modulation of dopamine

- D1 and adenosine A2A receptor signaling in the neostriatum. *Neuroscience* 2006;**141**:19–25.
- Sorkin LS, Maruyama K, Boyle DL, Yang L, Marsala M, Firestein GS. Spinal adenosine agonist reduces c-fos and astrocyte activation in dorsal horn of rats with adjuvant-induced arthritis. *Neurosci Lett* 2003; 340:119—22.
- 40. Wang S, Neel AI, Adams KL, Sun H, Jones SR, Howlett AC, et al. Atorvastatin differentially regulates the interactions of cocaine and amphetamine with dopamine transporters. *Neuropharmacology* 2023; 225:109387.
- Qie X, Wen D, Guo H, Xu G, Liu S, Shen Q, et al. Endoplasmic reticulum stress mediates methamphetamine-induced blood—brain barrier damage. Front Pharmacol 2017;8:639.
- 42. ElSohly MA, Slade D. Chemical constituents of marijuana: the complex mixture of natural cannabinoids. *Life Sci* 2005;**78**: 539–48
- Hao EK, Mukhopadhyay P, Cao ZX, Erdélyi K, Holovac E, Liaudet L, et al. Cannabidiol protects against doxorubicin-induced cardiomyopathy by modulating mitochondrial function and biogenesis. *Mol Med* 2015;21:38–45.
- 44. Valvassori SS, Bavaresco DV, Scaini G, Varela RB, Streck EL, Chagas MH, et al. Acute and chronic administration of cannabidiol increases mitochondrial complex and creatine kinase activity in the rat brain. Rev Bras Psiquiatr 2013;35:380–6.
- Chandra R, Engeln M, Schiefer C, Patton MH, Martin JA, Werner CT, et al. Drp1 mitochondrial fission in D1 neurons mediates behavioral and cellular plasticity during early cocaine abstinence. *Neuron* 2017; 96:1327–41.
- Sadakierska-Chudy A, Frankowska M, Filip M. Mitoepigenetics and drug addiction. *Pharmacol Ther* 2014;144:226–33.
- Khodamoradi M, Tirgar F, Ghazvini H, Rafaiee R, Tamijani SMS, Karimi N, et al. Role of the cannabinoid CB1 receptor in methamphetamine-induced social and recognition memory impairment. *Neurosci Lett* 2022;779:136634.
- Spiller KJ, Bi Gh, He Y, Galaj E, Gardner EL, Xi ZX. Cannabinoid CB1 and CB2 receptor mechanisms underlie cannabis reward and aversion in rats. Br J Pharmacol 2019;176:1268–81.
- Bisogno T, Hanuš L, De Petrocellis L, Tchilibon S, Ponde DE, Brandi I, et al. Molecular targets for cannabidiol and its synthetic analogues: effect on vanilloid VR1 receptors and on the cellular uptake and enzymatic hydrolysis of anandamide. *Br J Pharmacol* 2001; 134:845-52.
- Swenson KS, Wulschner LGE, Hoelscher VM, Folts L, Korth KM, Oh WC, et al. Fetal cannabidiol (CBD) exposure alters thermal pain sensitivity, problem-solving, and prefrontal cortex excitability. *Mol Psychiatr* 2023;28:3397–413.
- Huang J, Fan X, Jin XQ, Jo S, Zhang HB, Fujita A, et al. Cannabidiol inhibits Nav channels through two distinct binding sites. *Nat Commun* 2023:14:3613.
- Rosenberg EC, Chamberland S, Bazelot M, Nebet ER, Wang XH, McKenzie S, et al. Cannabidiol modulates excitatory—inhibitory ratio to counter hippocampal hyperactivity. *Neuron* 2023;111: 1282–300.
- Linden R, Esposito G, Scuderi C, Valenza M, Togna GI, Latina V, et al. Cannabidiol reduces Aβ-induced neuroinflammation and promotes hippocampal neurogenesis through PPARγ involvement. PLoS One 2011:6:e28668.
- Dou Y, Wu HJ, Li HQ, Qin S, Wang YE, Li J, et al. Microglial migration mediated by ATP-induced ATP release from lysosomes. Cell Res 2012;22:1022-33.
- 55. Koyanagi S, Kusunose N, Taniguchi M, Akamine T, Kanado Y, Ozono Y, et al. Glucocorticoid regulation of ATP release from spinal astrocytes underlies diurnal exacerbation of neuropathic mechanical allodynia. *Nat Commun* 2016;7:13102.
- Lin S, Huang L, Luo ZC, Li X, Jin SY, Du ZJ, et al. The ATP level in the medial prefrontal cortex regulates depressive-like behavior *via* the medial prefrontal cortex—lateral habenula pathway. *Biol Psychiatry* 2022;92:179—92.

 Pougnet JT, Toulme E, Martinez A, Choquet D, Hosy E, Boué-Grabot E. ATP P2X receptors downregulate AMPA receptor trafficking and postsynaptic efficacy in hippocampal neurons. *Neuron* 2014;83:417–30.

- Badimon A, Strasburger HJ, Ayata P, Chen XH, Nair A, Ikegami A, et al. Negative feedback control of neuronal activity by microglia. *Nature* 2020;586:417–23.
- Lazarevic V, Yang Y, Flais I, Svenningsson P. Ketamine decreases neuronally released glutamate via retrograde stimulation of presynaptic adenosine A1 receptors. Mol Psychiatr 2021;26:7425–35.
- 60. Hobson BD, O'Neill CE, Levis SC, Monteggia LM, Neve RL, Self DW, et al. Adenosine A1 and dopamine d1 receptor regulation of AMPA receptor phosphorylation and cocaine-seeking behavior. *Neuropsychopharmacology* 2013;38:1974–83.
- 61. Shahveisi K, Abdoli N, Khazaie H, Farnia V, Khodamoradi M. Maternal sleep deprivation affects extinction and reinstatement of methamphetamine reward memory in male offspring: role of the D1-like and D2-like dopamine receptors. *Brain Res* 2022;1792:148033.

- Bateup HS, Svenningsson P, Kuroiwa M, Gong S, Nishi A, Heintz N, et al. Cell type-specific regulation of DARPP-32 phosphorylation by psychostimulant and antipsychotic drugs. *Nat Neurosci* 2008;11:932–9.
- 63. Beck SJ, Guo L, Phensy A, Tian J, Wang L, Tandon N, et al. Deregulation of mitochondrial F1FO-ATP synthase *via* OSCP in Alzheimer's disease. *Nat Commun* 2016;7:11483.
- **64.** Nakano M, Imamura H, Sasaoka N, Yamamoto M, Uemura N, Shudo T, et al. ATP maintenance *via* two types of ATP regulators mitigates pathological phenotypes in mouse models of Parkinson's disease. *EBioMedicine* 2017;**22**:225–41.
- 65. Song L, Huang L, Luo ZC, Li X, Z.J. Du SY Jin, et al. The ATP level in the medial prefrontal cortex regulates depressive-like behavior *via* the medial prefrontal cortex—lateral habenula pathway. *Biol Psychiatry* 2022;**92**:179—92.
- 66. Trigo JM, Soliman A, Quilty LC, Fischer B, Rehm J, Selby P, et al. Nabiximols combined with motivational enhancement/cognitive behavioral therapy for the treatment of cannabis dependence: a pilot randomized clinical trial. *PLoS One* 2018;13:e0190768.